Published in: Philosophical Magazine, 2005, Vol. 85, pp 1395-1417

Room temperature precipitation in quenched Al-Cu-Mg alloys: a model for the reaction kinetics and yield strength development.

M. J. Starink † ‖ , N. Gao† , L. Davin‡ , J. Yan† , A. Cerezo‡

† Materials Research Group, School of Engineering Sciences, University of Southampton, Southampton, SO17 1BJ, United Kingdom

‡ Department of Materials, University of Oxford, Parks Road, Oxford OX1 3PH, United Kingdom

Abstract

The microstructural evolution during low temperature ageing of two commercial purity alloys (Al-1.2Cu-1.2Mg-0.2Mn and Al-1.9Cu-1.6Mg-0.2Mn at.%) was investigated. The initial stage of hardening in these alloys is very rapid, with the alloys nearly doubling in hardness during 20 h ageing at room temperature. The microstructural evolution during this stage of hardening was investigated using differential scanning calorimetry (DSC), isothermal calorimetry and three-dimensional atom probe analysis (3DAP). It is found that during the hardening a substantial exothermic heat evolution occurs and that the only microstructural change involves the formation of Cu-Mg co-clusters. The kinetics of cluster formation is analysed and the magnitude of the hardening is discussed on the basis of a model incorporating solid solution hardening and modulus hardening originating from the difference in modulus between Al and clusters.

‖ Author for correspondence: Tel: 023 80595094; Fax: 023 80593016;

Email:M.J.Starink@soton.ac.uk

1. Introduction

Al-Cu-Mg based alloys (2xxx series) are widely used in structural applications, in particular alloys with Cu:Mg atomic ratio close to 1 are used extensively in the aerospace sector, whilst alloys with low Cu content (0.1-0.25at%) and 3 to 4 at%Mg are thought to be potential alloys for car body applications. It has been found that hardening occurs in two distinct stages in Al-Cu-Mg alloys (Hardy 1954-55, Vietz and Polmear 1966, Takahashi and Sato 1985), with the first stage of age hardening leading to a plateau stage during which ageing causes no further hardening. The first stage of hardening occurs within about 1 minute ageing for ageing temperatures between about 100 and 200°C. Also ageing at room temperature causes the hardness to reach a plateau, and it is generally thought that both hardening reactions are due to the same mechanism. In studies on Al-Cu-Mg based alloys with and without micro alloying additions or impurities and with a range of Cu:Mg ratios, several explanations for the first stage of hardening were suggested. The main four mechanisms are strengthening due to I) GP (Guinier-Preston) or GPB (Guinier-Preston-Bagaryatski) zone formation, II) co-cluster formation, III) locking of existing dislocations due to a solute-dislocation interaction and IV) formation of a S" phase.

Mechanism I, GP/GPB zone hardening, has been invoked in many works through out the 1950s to mid 1990s (Silcock 1960-61, Vietz and Polmear 1966) and later (Zahra *et al*. 1998, Charai *et al*. 2000). (We are adopting the definition of zones given by Sato (2000), i.e. a zone differs from a cluster in the sense that a zone has a distinct shape and is larger than about 2nm.) However, several works (Ringer *et al*. 1996 and 1997b) have reported that no zones can be observed at this early stage of ageing. Instead Ringer *et al.* (1997a, 1997b) reported that in a high purity Al-1.1at%Cu-1.7at%Mg alloy Cu/Mg sub-nanometer clusters have been observed after a short ageing time (within

5 min at 150°C) by means of conventional atom probe field ion microscopy (APFIM) and proposed that the initial rapid hardening is due to these clusters (Ringer *et al*. 1997a, 1997b) (mechanism II). According to this work the second stage (the peak of hardness) is due to GPB zone formation.

Reich *et al.* (1999) considered a somewhat different mechanism for hardening suggesting that it was caused by solute-dislocation interactions (mechanism III). In this mechanism Cu and Mg solute atoms segregate to the dislocations present from before the hardening, locking these dislocations and increasing the hardness. This suggestion was based on three main observations from experiments in a high purity Al-1.1at%Cu-1.7at%Mg alloy: i) no clusters were observed by three-dimensional atom probe (3DAP) analysis within 1 min at 150ºC (corresponding to rapid hardening stage), ii) further rapid hardening occurred following deformation after ageing, iii) decoration of dislocations by S precipitates and precipitate free zones around the dislocations (dislocation loops) both observed later in the precipitation process suggested that Cu and Mg atoms cluster around dislocations in the early stage of ageing. Coincidence Doppler broadening of positron annihilation radiation data has been interpreted (Nagai *et al*. 2001) as suggesting that at 150°C vacancy–Mg complexes rapidly migrate to vacancy sinks and vacancy–Mg–Cu complexes form along dislocations during the first 1 min aging. This indirect evidence was considered to support the dislocation–solute interaction (mechanism III) as the origin of the initial rapid hardening. It was proposed that whilst a uniform dispersion of Cu-Mg co-clusters does occur, it only occurs after the first rapid hardening, and are thus not responsible for the initial hardening. Ratchev *et al.* (1998, 1999) have found a similar two-stage age hardening curve in a commercial purity Al–4.7at%Mg–0.3at%Cu alloy and they attributed the initial hardening stage mainly to heterogeneous formation of a phase termed S" phase on dislocation helices (mechanism IV).

The works cited above refer mostly to high purity Al-Cu-Mg alloys. It is conceivable that the reaction is to some extent influenced by the presence of small amounts of additional alloying elements or impurities, such as Si (Raviprasad *et al.* 2003), Fe or Mn. This could somewhat influence the relative importance of the mechanisms. As commercial aluminium based alloys will always contain some Si and Fe, with grain structure controlling additions such as Mn (Li *et al.* 2001, Gao *et al.* 2002), and in the case of the widely used AA2024 (Al-Cu-Mg-Mn) are generally aged at room temperature, it was decided to perform a detailed study of microstructural changes in the course of the hardening in commercial purity Al-Cu-Mg-Mn alloys. The techniques applied are isothermal calorimetry, differential scanning calorimetry (DSC) and 3DAP.

Following on from the analysis of the microstructure and microstructural development, the main aim of the present work is to analyse the new microstructural data and to investigate the potential for a physically based quantitative model for the rapid hardening that can generalise the observations, and that can be applied to quantitatively predict hardening in these alloys. The approach proposed here derives from methodologies that have proved successful in providing accurate models for precipitation hardening in several alloy systems (Starink *et al.* 1999, Liu *et al.* 2003, Esmaeili 2003, Starink and Wang 2003), and involves some simplifications of the precipitation kinetics and dislocation-precipitate interactions. Thus, rather than attempting to provide a definitive analysis of the structure of the precipitates that are responsible for the hardening, we aim to provide a reasonable, simplified model describing the average microstructural parameters during ageing, leading to an accurate model for strengthening that provides predictive capability.

2. Experimental procedures

Two commercial purity Al-Cu-Mg-Mn alloys with Cu:Mg ratio close to 1 (atomic ratio) have been studied, the compositions are reported in table 1. For all alloys, 99.90wt% aluminium was used as base to ensure comparable, low impurity contents, and Fe and Si contents of the alloys are expected to be between 0.02 and 0.04at%. The production route included casting, stress relieve at 300°C /24 h, homogenizing for 24 h, upset forge, hot rolling to 20 mm plate at ~420°C, solution heat treatment, cold water quench and stretch by 2.5%. To remove dislocations and to dissolve (pre-) precipitates generated in previous processing and ageing, all samples were freshly solution treated at 495°C and subsequently quenched into water at room temperature before the ageing treatments commenced. Room temperature ageing was performed at about 25°C and for ageing at 50°C, samples were transferred to an air circulation furnace within 5 seconds from completion of the quench.

[Insert table 1 above here]

Age hardening was studied by performing Vickers hardness tests on quenched and naturally aged specimens. The hardness values were obtained from surfaces ground with #1200 grade SiC-paper. Four indentations were made on each specimen with a 20kg load and a mean hardness is reported. For the Al-1.9Cu-1.6Mg alloy additional verification experiments were performed and the average hardness from two specimens is reported.

Samples aged at room temperature and at 50°C were studied in a Perkin-Elmer Pyris 1 calorimeter. Samples were discs (5 mm diameter and approximately 1 mm thickness) that were machined prior to solution treatment. For linear heating experiments the samples were introduced into the DSC held at 0°C within 2 min after completion of the preceding heat treatment. DSC runs were started immediately after introduction of the sample. Scanning over the temperature range 5-540°C at a

constant heating rate of 10°C/min was performed. To correct for baseline drift and heat capacity of the sample and reference (Starink 2004), a two stage baseline correction was performed. First a DSC run with empty pans was subtracted from the data. Secondly, the data was corrected by assuming that the combined effect of heat capacity differences and baseline fluctuations results in a heat flow which is a second order polynomial. The coefficients were fitted by assuming that the heat effects due to reactions are zero at three temperatures: 40, 120 and 498°C.

For isothermal calorimetry experiments samples were introduced into the Pyris 1 calorimeter within 3 min after quenching and immediately heated to 25 or 50°C, where they were held for up to 24 h. Baseline corrections were performed by subtracting an exponentially decaying heat flow with half time determined from a calorimetry experiment that was conducted on a pure aluminium sample, and a further constant heat flow was added to ensure that heat flows were exothermic. During the first 30 to 60 s after heating to the isothermal ageing temperature, the heat flows are unstable because the apparatus is equilibrating, and this part of the calorimetry experiment is neglected.

The 3DAP analyses were conducted using an energy-compensated optical position sensitive atom probe. The specimens in the shape of sharp needles with an end radius less than 100 nm were prepared by a two-stage electropolishing method. Analyses were carried out at 15 K with a pulse fraction (ratio of the pulse voltage to the direct current standing voltage) of 20% and a pulse repetition rate of 1500 Hz. The voltage was between 4.5 and 9.5 kV depending on the analysis. The tips have been made after solution treatment at 495ºC except the specimens for the shortest time of ageing at 25ºC (e.g. 15 min and 30 min). In those cases the tips were made before the solution treatment in order to allow quick transfer to the atom probe. To avoid loss of solute (particularly Mg) from the region of analysis, the drop polishing (Miller 2000) was used to form a point as far back from the original end as possible. For selected experiments, the tips were enclosed in a box

constructed of the Al-1.9Cu-1.6Mg alloy during solution treatment. Analyses where the measured solute content was significantly below the nominal value were discarded.

3. Results and analysis

3.1 Hardness

The hardness evolution during ageing at 25°C of solution treated samples shows a rapid increase in hardness for both samples (figure 1). The hardness values in the freshly quenched condition are 72 for the Al-1.2Cu-1.2Mg alloy and 91 for the Al-1.9Cu-1.6Mg alloy. As we may approximate the yield strength in MPa of these underaged aluminium alloys as about 2.3 times the Vickers hardness value (Starink *et al.* 2002), it is clear that the hardness / strength after a few minutes at room temperature is already substantial.

[Insert figure 1 above here]

3.2 3DAP analysis

In contrast to samples aged at 150°C (Gao *et al.* 2002) no precipitates or structures reminiscent of GPB zones have been observed by 3DAP in any of the samples during or after the room temperature hardening, but we did identify clustering of solute atoms. The clustering was identified using the statistical procedure of frequency distribution analysis (Miller and Smith 1988). In this procedure, the frequency distribution is obtained by plotting the number of blocks containing a given number of atoms of a particular type (Mg or Cu) against this given number. An example for the analysis of the

Al-1.2Cu-1.2Mg alloy aged at room temperature for 2h is shown in figure 2(a). The observed distribution is compared to a binomial distribution representing a random distribution using the χ^2 test. The null hypothesis is therefore a case where there is no clustering of Mg or Cu atoms. An atomic distribution is taken to be non-random if the probability of obtaining the measured χ^2 value is 5% or less (95% confidence limit). To check the consistency of the test, the number of atoms per block is varied from 100 to 400.

Figure 2(b) shows that for the Al-1.2Cu-1.2Mg alloy, the distribution of Mg atoms is random up to 1h ageing at room temperature and non random after 2h. This suggests that the onset of clustering happens between 1h and 2h. Similar results have been found for the Al-1.9Cu-1.6Mg alloy. However, for this alloy the period of transition between random and non-random distribution seems shorter. Results concerning specimens aged at room temperature for 30 min show a random distribution of the Mg atoms but after 1h the distribution is found to be non-random.

[Insert figure 2 above here]

For the Al-1.9Cu-1.6Mg alloy, the results show that the distribution of the Cu atoms is non-random even for the shortest time (e.g. 15 min) of natural ageing. For the Al-1.2Cu-1.2Mg alloy the distribution of Cu atoms is found to be non-random after 1h at room temperature. The results of the test for a specimen quenched and aged at room temperature for 30 min are inconclusive, with the chi-square probability depending on the number of atoms per block. We thus consider that this stage marks the onset of the clustering of Cu atoms. It can be concluded that for the Al-1.9Cu-1.6Mg alloy, the clustering of Cu atoms occurs after a very short time at room temperature or even during quenching. For the Al-1.2Cu-1.2Mg alloy, the clustering of Cu atoms seems somewhat slower and occurs only after about 30 min at room temperature.

The atom map from a 3DAP analysis of the Al-1.2Cu-1.2Mg alloy aged at 25ºC for 2h is shown in figure 3(a) (More 3DAP data on both alloys is provided in Gao *et al.* 2002 and Davin 2004). Although the frequency distribution clearly shows the non-randomness of Cu and Mg atoms in the alloy, there is no indication of the presence of any particles with a distinct shape, such as GP/GPB zones, so the results must be due to very small clusters that are not visible in the atom map. To study the density and composition of the clusters formed, the maximum separation method has been used (Miller 2000, Vaumousse *et al.* 2003). In this procedure, the selection of solute-rich regions is performed by connecting solute atoms (in our case Cu and Mg), which lie within a fixed distance (d), and eliminating clusters containing less than a minimum number of solute atoms (N_{min}). Other atoms within some distance L greater than d are taken to belong to the cluster. To fix these values a random distribution of the same composition was simulated by using the same positions as the experimental data but randomly assigning these positions to the detected elements. In such a random distribution, no (or few) clusters are expected if the parameters are well-adjusted. The values of d and L have been fixed at 0.5 and 0.55 nm respectively and the minimum number of atoms forming a cluster has been fixed at 6 for the Al-1.2Cu-1.2Mg alloy and 7 for the Al-1.9Cu-1.6Mg alloy. An example of the spatial distribution of the clusters is given in figure 3(b). The measured value of cluster density will obviously depend on the parameters selected and is subject to significant errors due to the limited number of clusters (1 to 29) detected in any one analysis. Nonetheless, this method allows an estimate of the cluster density to be made and also gives an indication of the trends with ageing time. The density in clusters has been found to vary from 7×10^{22} to 4×10^{23} clusters per m^3 for the Al-1.2Cu-1.2Mg alloy (figure 4(a)). The maximum in density is reached after 3.5h of heat treatment at 25ºC and for longer times the density stays stable or decreases slightly. For the Al-1.9Cu-1.6Mg alloy, the density in clusters is higher whatever the time of natural ageing (figure 4(b)). It varies approximately from 3×10^{23} per m^3 after 15min to 8×10^{23} per

m^3 after only 1h of ageing at 25ºC. This difference in density compared to the first alloy can be explained mainly by the higher solute content in the Al-1.9Cu-1.6Mg alloy.

[Insert figures 3 and 4 above here]

The compositions of the clusters have been calculated by taking the total number of Mg and Cu atoms involved in clusters in the experimental dataset and subtracting the total number of Mg and Cu atoms from the clusters found in the corresponding random dataset. It was observed that for all samples in which the distribution of both elements is non-random, the composition of clusters is variable, but clusters that are predominantly rich in one of the two elements form a small minority of the total number of clusters. Thus clusters are predominantly Cu-Mg co-clusters. Figures 5(a) and (b) show the average solute content in the clusters found in specimens naturally aged between 15 min and 48h. In both alloys, the clusters become enriched in Mg as the time of natural ageing increases. In the case of the Al-1.2Cu-1.2Mg alloy, this enrichment is particularly noticeable between 1h and 2h with the Mg content increasing from 32.1±1.9% to 78.3±1.5%. For the Al-1.9Cu-1.6Mg alloy the average composition of the clusters aged at 25ºC for 15 min are nearly pure Cu but the Mg content increase dramatically after 30 min of natural ageing. After a long period of time at 25ºC, the content in Cu stays close to 40%. These results are consistent with the measured non-random Cu distribution from very early stages, with Mg distributions only becoming non random after some natural ageing. In addition, the variation in composition is limited among the clusters found in a same dataset which means that as the time of ageing gets longer Mg is co-clustering with the Cu clusters formed at early stages and the formation of Mg-Mg clusters may be very limited. The results show that whatever is the time of natural ageing or the alloy, the variations of the Al content in the clusters are low. The average Al content in the Al-1.2Cu-1.2Mg alloy is 92.3±0.2% and in the Al-1.9Cu-1.6Mg, 91.2±0.1%. However it should be noted that the lateral

resolution of the 3DAP is approximately 0.5nm and this together with the method used for grouping the atoms belonging to the cluster is likely to give a matrix contribution to the measurement. These values should therefore be taken as upper limits.

[Insert figure 5 above here]

In several works it has been considered that the binding energy between Mg atoms and vacancies is higher than that between Cu atoms and vacancies (Ozbilen and Flower 1989, Beatrice *et al.* 1995) and that the activation energy for Mg diffusion in an Al alloy is lower than for Cu diffusion (Zahra *et al.* 1990). It has been suggested that this would indicate that Mg-Mg clusters are the first type of clusters to appear followed by Cu-Mg and Cu-Cu clusters (Charai *et al.* 2000) and that lattice parameter measurements performed on an Al-Cu-Mg alloy during natural ageing (Rajan 1973) would support that sequence of cluster formation. However, our 3DAP data clearly show that for our present commercial purity Al-Cu-Mg based alloys indicate that Cu clusters form before the Mg atoms cluster.

3.3 Calorimetry

Figure 6 presents the heat flow during isothermal ageing at 25 and at 50°C as measured using isothermal calorimetry. This figure reveals that a single exothermic heat effect occurs during this low temperature ageing. For both alloys, the time interval for heat evolution coincides with the time interval for the increase in hardness and the time interval during which Mg clustering is observed by 3DAP, indicating that the Mg clustering forming co-clusters is the reaction responsible for both the heat evolution and the rapid hardening. The isothermal calorimetry data shows that the cluster

formation reaction is slower in the more dilute Al-1.2Cu-1.2Mg alloy. This is consistent with the 3DAP data.

[Insert figure 6 above here]

DSC curves for the Al-1.9Cu-1.6Mg alloy after ageing at 25°C are presented in figure 7. Four effects (two exothermic and two endothermic), numbered I to IV, are evident. Effects III and IV are discussed in detail elsewhere (Gao *et al.* 2002, Starink *et al.* 2002); they can be identified as due to S phase formation (effect III, in the range of 230-320°C with a peak at about 270°C) and S phase dissolution (effect IV, in the range of 330-470°C). These effects are of no direct concern to us here as they are unrelated to ageing at 25 and 50°C. In the literature (Jena *et al.* 1989, Luo *et al.* 1993) many suggestions concerning the origin of effect I have been made and various terms have been used to identify the structures formed in this exothermic reaction (GP or GPB zones, GPB I / GPB II zones, clusters). Our 3DAP results clearly show that effect I should be ascribed to the formation of clusters. It is known that the clusters are still present after ageing at 150°C for several hours and that the clusters will become unstable at about 190°C (Gao *et al.* 2002, Starink *et al.* 2002). Hence the endothermic effect II is thought to be due to the dissolution of the clusters. We also performed DSC experiments on the Al-1.2Cu-1.2Mg alloy aged for various times at room temperature (Starink *et al.* 2004a) and on both alloys after ageing for various times at 50°C. This showed that at both temperatures the reduction of the cluster formation effect, effect I, with ageing time is slower in the more dilute Al-1.2Cu-1.2Mg alloy. Thus also the DSC data confirms that cluster formation is slower in the more dilute Al-1.2Cu-1.2Mg alloy.

[Insert figure 7 above here]

4. Discussion

4.1 The mechanisms of room temperature hardening

In attempting to devise a model that can generalise the observations and have predictive capability, it is noted that the present results show that the exothermic heat release on ageing coincides with the hardness increase during ageing which in turn coincides with the formation of Cu-Mg clusters, whilst no GPB zones or S phase is detected at this stage. The present results indicate that there is no evidence that mechanisms I and IV contribute to the room temperature hardening. In a preliminary assessment of literature data and tensile tests (Starink *et al.* 2004a) we highlighted several reasons which lead us to believe that Cu-Mg co-cluster formation (mechanism II) is the dominating factor for room temperature age hardening of our alloys. Firstly, ageing-deformation-ageing cycles at room temperature on the commercial purity Al-1.9Cu-1.6Mg alloy (Starink *et al.* 2004a) do not show the age hardening after deformation that led Reich *et al.* (1999) to propose mechanism III for their high purity Al-1.1at%Cu-1.7at%Mg alloy aged at 150°C. Secondly, the heat release that coincides with the room temperature strengthening is of similar order of magnitude as the heat effect due to S phase formation (see figure 7), and hence it is likely that a pre-precipitate is formed. Thirdly, on a (shear) plane through the material the inter-loop spacing of dislocations is in the order of 100nm (Reich *et al.* 1999, Nagai *et al*. 2001) whilst the spacing for fine precipitates formed in artificially aged high purity Al-Cu-Mg (Reich *et al.* 1999), Al-Cu-Mg-Ag-Si (Raviprasad *et al.* 2003), commercial purity Al-Cu-Mg and Al-Cu-Mg-Li (Starink *et al.* 1999a) is almost an order of magnitude smaller but the strengthening increment due to the formation of these precipitates is generally similar to that of the rapid hardening or room temperature age hardening. Thus it is unlikely that dislocation loops with solute gathering around it can provide a major contribution to

age hardening. In addition, quenched Al-Mg-Cu alloys with low Cu:Mg ratio aged at about 170°C show rapid hardening but do not show dislocation loops (Starink *et al.* 2004). Hence for these alloys mechanism III is definitely not possible.

Apart from these considerations pointing away from mechanism III, a further practical problem is that that currently no model is available to quantitatively describe hardening due to mechanism III. Thus, the purpose of the present discussion is to investigate whether the room temperature ageing in our alloys can be quantitatively described by hardening due to the formation of Cu-Mg co-clusters. In the following we will specifically consider that strengthening by the Cu clusters present a few minutes after quenching to be limited, with all age hardening due to the formation of Cu-Mg clusters with fixed Cu:Mg ratio, here the Cu:Mg ratios are taken to be 1:1.

In a first assessment we consider that strengthening due to (co-)clusters may be due to three mechanisms i) order strengthening and stacking fault strengthening, ii) chemical hardening and iii) modulus hardening. As selected area diffraction of Al-Cu-Mg alloys aged to just after the initial increase in hardness (i.e. just after the completion of co-cluster formation) do not show any distinct evidence of additional diffraction effects, it is believed that at this stage co-clusters have no internal order. Hence, at this stage, order strengthening or stacking fault strengthening can not occur, and the long plateau stage indicates that even if some limited ordering may occur later (for instance if GPB2 structures form) order strengthening and stacking fault strengthening is very limited. Chemical hardening, in a classical sense, occurs when the cutting of precipitates by a dislocation creates additional matrix-precipitate interface area. This mechanism can be analysed if there is a well defined matrix-precipitate interface with a clearly-defined interfacial energy, but cluster-matrix interfaces are diffuse and interfacial energy is probably very small. If chemical hardening plays a significant role, we would expect serrated yielding to occur due to repeated shearing and

reformation of clusters. But examination of a range of published data on Al-Cu-Mg alloys aged to the plateau stage (Starink *et al.* 2004a, Yan *et al.* 2004) shows that this is generally not observed. Hence, it is both reasonable and practical to start the analysis by assuming that chemical hardening is relatively small, and concentrate on modulus hardening only. The validity of neglecting any potential contribution due to chemical hardening then needs to be tested by considering the accuracy of the model predictions.

We aim to produce a model that can not only describe final hardening, but also model the hardness in the course of the age hardening process, and hence we will first derive a model for the formation rate of clusters. This is the aim of section 4.2, with the subsequent section 4.3 focussing on the strength of the alloys during the cluster formation reaction.

4.2 The kinetics of cluster formation

The kinetics of formation of clusters is an atomic scale process that involves the interaction between Al, Cu and Mg atoms and vacancies. Rather than attempting to fully capture the atomic scale effects involved, which is unlikely at this stage to lead to a model with the predictive capabilities we aim for, we will investigate the kinetics of Cu-Mg cluster based on a model of nucleation, growth and impingement of diffusion fields considers averaged properties such as averaged nucleation rates, average solute content of the Al rich phase and average size. The approach is in part based on the treatment for deriving the Johnson-Mehl-Avrami-Kolmogorov method (Avrami 1939, 1940, 1941, Cumbrera 1995, Sessa 1996); the full derivation of the present method and comparison with experimental data is provided elsewhere (Starink and Zahra 1997a, 1998a, b, Starink *et al.* 1998). In brief, the effective transformed volume, V_P, around a single nucleus is considered to grow according to:

$$V_p = A\,[G\,(t\text{-}z)]^m \tag{1}$$

where G is the (average) growth rate, A is a constant, z is the time at which the nucleus is formed, whilst m is a constant related to the dimensionality of the growth and the mode of transformation, termed the growth exponent. Precipitates will grow by diffusion-controlled growth in 3 dimensions, and for this m=1½ (Starink 2004). The extended transformed fraction $\alpha_{ext} = V_{ext}/V_o$, where V_o is the volume of the sample, is given by:

$$\alpha_{ext} = \int_0^t AI(z)\left[G(t-z)\right]^m dz \tag{2}$$

The growth rate G and the nucleation rate I can be approximated by Arrhenius type temperature dependencies with activation energies E_G and E_N. Introducing the impingement exponent η_i (Starink 2001) provides the equation for the fraction transformed, α:

$$\alpha = 1 - \left(\frac{\alpha_{ext}}{\eta_i} + 1\right)^{-\eta_i} \tag{3}$$

For isothermal paths, the nucleation rate, $I(z,T)$, will generally be constant or zero. The latter case arises for the limit of $I(z)$ decreasing infinitely fast, and it can, for instance, occur when the number of nucleation sites is limited and all sites are used for nucleation very early on in the transformation (so-called 'site saturation'). For both cases a single general expression can be derived (Starink and Zahra 1997a, 1998b):

$$\alpha_{ext} = [k(T)\, t]^n \tag{4}$$

where $k(T)$ is a temperature dependent factor determined by A, G and I, or (for the site saturation case) A, G and the density of nuclei. Through integration of equation (2) it can be shown that for constant nucleation rate $n = m + 1$, whilst for zero nucleation rate $n = m$ (Cumbrera and Sanchez-Bajo 1995, Starink and Zahra 1997a, 1998b). Both cases have been observed for precipitation reactions in various Al based alloys (Starink and Zahra 1997a, 1998b, Starink *et al.* 1998, 1999b). We will take $k(T)$ as:

$$k(T) = k_o \exp\left[-\frac{E_{eff}}{RT}\right] \tag{5}$$

where E_{eff} denotes the effective activation energy for the experiments, R is the gas constant, k_o is a constant. Assuming that both the growth rate and the nucleation rate can be described by Arrhenius type dependencies, α_{ext} for linear heating can be approximated very accurately as (Starink and Zahra 1997a, 1998b, Starink 2003, 2004):

$$\alpha_{ext} \cong \left(\frac{\beta k_B}{E_G} k_c \exp\left[\frac{-E_{eff}}{RT}\right] \left(\frac{T}{\beta}\right)^2 \right)^s \tag{6}$$

where

$$E_{eff} = \frac{mE_G + E_N}{m+1} \tag{7}$$

$$s = m + 1 \tag{8}$$

where β is the heating rate, and k_C is a constant. Also for the case where nuclei are present before the start of the transformation and no further nucleation occurs, equation (6) is a good approximation. In this case $s = m$ and $E_{eff} = E_G$. This, in combination with equation (8), shows that if the assumptions for the derivation of equations (6) to (8) are satisfied and the processes occurring for an isothermal and a linear heating path are the same, *s* equals *n*.

The activation energy for cluster formation was obtained from DSC curves of a commercial 2024 alloy at three heating rates (5, 10 and 20°C/min) using the three most accurate isoconversion methods described in (Starink 1996, 2003). No significant variations between the different isoconversion methods were observed and the average value was E = 75 kJ mol^{-1}. The reaction exponent *s* was determined from the DSC data using the method described in (Starink and Zahra 1997b) and results are presented in figure 8. This figure shows that *s* decreases from an initial value of about 2.5 to about 0.5 at the stage where the Cu-Mg cluster formation is virtually completed. The initial value for *n* of 2.5 indicates that in samples that have undergone very limited ageing at room temperature, Cu-Mg cluster formation during the subsequent DSC run is a nucleation and growth process with continuous nucleation. In combination with the 3DAP results, the observation of continuous nucleation indicates that whilst Cu-Mg clusters might form on pre-existing Cu clusters, the amount of pre-existing clusters is not a limiting factor for the reaction. (If the amount of nucleation sites would be exhausted early in the transformation, *s* would equal 1½.) A decreasing value of *s*, as observed in figure 8, is in line with transformation theory (Starink and Zahra 1997a, 1998a, b), and indicates that when substantial amounts of Cu-Mg clusters have formed during isothermal ageing, the subsequent additional Cu-Mg cluster formation during the DSC run occurs by growth of these pre-existing Cu-Mg clusters. Following transformation theory (Starink and Zahra 1997a, 1998a, b), the final value of *s* of 0.5 corresponds to the case where Cu-Mg cluster formation during the DSC run occurs by growth of Cu-Mg clusters substantial initial size. (In this case the

diffusion process leading to precipitation during the DSC run can be approximated as a 1 dimensional diffusion problem (Starink and Zahra 1998b), and has been observed before for DSC experiments on pre-aged samples (Starink and Zahra 1998a)). We also applied the kinetics model described above (i.e., equations (3) and (6)) to fit the Cu-Mg cluster formation effect in DSC curves obtained from the Al-1.2Cu-1.2Mg and the Al-1.9Cu-1.6Mg alloy aged at 25°C, and similar values for s were observed. Figure 9 shows a very good agreement between experiment and fitted model for the Al-1.2Cu-1.2Mg alloy aged at 25°C for 0.08h (5 min). This best fit gives the reaction exponent s = 2.42, the impingement parameter η_i =0.36 (activation energy was again fixed at 75 kJ mol^{-1}).

[Insert figures 8 and 9 above here]

In attempting to verify the above kinetic model through comparison with measured cluster densities presented in figure 4, we need to consider the main stages of classical nucleation and growth theory: nucleation, growth, impingement and coarsening. In the classical theory continuous nucleation implies that the nucleation rate is constant in the 'extended volume' (Starink 2001). This means that the real nucleation rate is initially constant, then decreases when substantial impingement sets in, and the number of clusters will ultimately reduce when coarsening sets in. The occurrence of substantial impingement can be identified with the first inflection point in the heat release, whilst the reduction in heat release after the peak indicates strong impingement which would be related to very limited or zero additional nucleation, and coarsening (i.e. dissolution of smaller clusters) can set in the latter stages of the heat release. Figure 4(a) shows that cluster density for the Al-1.2Cu-1.2Mg alloy first increases and then peaks between about 3 and 20 h, which is followed by a slight decrease in cluster density. This is consistent with the nucleation-growth-impingement-coarsening sequence if we consider that the peak in heat flow is observed after about 2 h (figure 6). Data for

the Al-1.9Cu-1.6Mg alloy (figure 4(b)) indicates the peak in cluster density is at about 1.5 to 5 h (the limited accuracy of cluster density measurement may have caused some fluctuations), whilst the peak in heat flow is observed at about 1.5h. Also here cluster density evolution is broadly consistent with the model and the calorimetry.

To model the kinetics of cluster formation in these two alloys, the model presented above is further developed to find an expression in which the dependence of the transformed fraction on temperature and concentration is included in an explicit form. Following the classical nucleation theory, the nucleation rate I is given by (Christian 1975):

$$I = N_0 Z \beta^* \exp\left(-\frac{\Delta G^*}{RT}\right) \tag{9}$$

where Q_d is the activation energy for diffusion of solute atoms, N_o is the number density of potential nucleation sites and ΔG^* is the activation energy barrier for homogeneous nucleation. I_0 is the pre-exponential factor related to the number of nucleation sites. I_0 depends on temperature and concentration, but not so strongly as the exponential term. In the classical nucleation theory the expressions for ΔG^*, Z and β^* are (Robson et al. 2003, Russell 1970):

$$\Delta G^* = \frac{16\pi\gamma^3}{3\Delta F_v^2} \tag{10}$$

$$Z = \sqrt{\frac{\Delta G^*}{3\pi k_B T}} \frac{V_{at}}{\frac{4}{3}\pi r^{*3}} \tag{11}$$

$$\beta^* = \frac{4\pi r^{*2} Dc}{a^4} \tag{12}$$

where γ is the interfacial energy, ΔF_v is the driving force per unit volume for precipitation, k_B is the Boltzman constant, V_{at} is the atomic volume, r^* is the critical radius for nucleation, D is the (temperature dependent) diffusion coefficient of solute atoms in matrix ($D = D_o \exp(-Q_D/RT)$, where Q_D is the activation energy for diffusion and D_o the pre-exponential factor), c is the concentration of solute atoms and a is the lattice parameter of the precipitate. For a dilute alloy, the activity of the alloying element can be replaced by its concentration, and the driving force ΔF_v can be written as [23]:

$$\Delta F_v = \frac{RT}{V_m} \ln\left(\frac{c}{c_e}\right) \tag{13}$$

where V_m is the molar volume, c_e is the equilibrium solute concentration in the matrix. Thus the activation energy barrier ΔG^* for nucleation is given by:

$$\Delta G^* = \frac{16\pi\gamma^3}{3\left[\frac{RT}{V_m}\ln\left(\frac{c}{c_e}\right)\right]^2} \tag{14}$$

By combining the above expressions (Eqs. 9-14) we can see that the nucleation rate can be effectively approximated as:

$$I \cong I_0 \exp\left(-\frac{\Delta G^* + Q_d}{RT}\right) \tag{15}$$

In which I_o is proportional to c and has a relatively weak temperature dependence as compared to the exponential term.

From the established equation for diffusion controlled growth the growth rate is given by:

$$G = \frac{c - c_e}{c_p - c_e}\frac{D}{r} = \frac{c - c_e}{c_p - c_e}\frac{D_0}{r}\exp(-\frac{Q_d}{RT}) = G_0 \exp(-\frac{Q_d}{RT}) \quad (16)$$

This shows that G_o is proportional $(c - c_e)$. Seeing that I_o is proportional to c and G_o is proportional $(c - c_e)$ whilst c_e is mostly much smaller than c, the rate constant $k(T)$ in equation (4) can be approximated accurately as:

$$k(T,c) \cong k_0(c - c_e)\exp(-\frac{E_{eff}}{RT}) \quad (17)$$

where

$$E_{eff} = \frac{mE_G + E_N}{m+1} = Q_d + \frac{\Delta G^*}{m+1} \quad (18)$$

The validity of these expressions was checked by fitting the isothermal calorimetry and DSC curves, and a good correspondence was found for γ = 0.06J m^{-2} with n=2.5 (figure 10). Thus the model describes $\alpha(t,T)$ well and the expressions will be used as part of a strengthening model described in the next section.

[Insert figure 10 above here]

The above treatment raises the question as to what an interfacial energy γ represents for the case of clusters, which in general do not have a clearly definable interface with the remaining matrix. We

propose that γ here should be interpreted as the proportionality constant which describes the dependency of the free energy change due to the formation of a cluster on the effective area, e.g. for a spherical cluster of effective size *r*:

$$\Delta G_{sc} = \frac{4}{3}\pi r^3 \Delta H - 4\pi r^2 \gamma \tag{19}$$

where ΔG_{sc} is the change in free energy due to the formation of a single cluster, ΔH is the enthalpy change per unit volume due to the formation of a cluster.

It is further noted that the consistent observation from the analysis of the different calorimetry experiments that cluster formation involves significant nucleation at least in the initial stages of the process, is in line with the measured cluster densities from 3DAP (figure 4). Also the predicted lower nucleation rate for the more dilute alloy is in line with the relative nucleation rates for the two alloys in figure 4.

4.3 A model for modulus hardening by clusters

Modulus hardening is fairly well understood conceptually (Nembach 1983, 1996, Ardell 1985), but very few descriptions have been quantitatively compared to experimental data. A description in which modulus hardening increases with increasing radius of the clusters, such as the one suggested in Ref (Nembach 1983), seems to be inappropriate for the present co-clusters as during coarsening a constant alloy hardness is observed. Here, we adopt the approximation for modulus hardening first proposed by Cartaud *et al.* (1976) and later applied in several works on rapid hardening of Al based

alloys (Gomiero *et al.* 1992, Starink *et al.* 1999a, 2004), which predicts a constant hardening effect during coarsening:

$$\Delta\tau_{cl} = \frac{\Delta\mu}{4\pi\sqrt{2}} f_{cl}^{1/2} \tag{20}$$

where $\Delta\mu$ is the difference between the shear moduli of the matrix, μ_m, and the clusters, μ_{cl}, f_{cl} is the volume fraction of the clusters. The shear modulus of the clusters in our alloys is unknown. It has been suggested that the shear modulus of clusters can be approximated as a weighted average of the moduli of the individual pure substances (Gomiero *et al.* 1992) and for the present Cu-Mg clusters this would mean:

$$\mu_{cl} = x_{Cu}\mu_{Cu} + x_{Mg}\mu_{Mg} + x_{Al}\mu_{Al} \tag{21}$$

where μ_{Cu}, μ_{Mg}, μ_{Al} are the shear moduli of Cu, Mg, Al and x represents the fraction of the respective atoms in the cluster. For the present clusters x_{Al} was determined as about 92% (upper limit estimate, see section 3.2), whilst x_{Mg} : x_{Cu} is about 1 (figure 5). Although the value obtained from the above equation may give an estimation of μ_{cl}, it is not thought to be a reliable estimate. (For example, the shear modulus of Al_3Li does not correspond to this type of estimate (Guo *et al.* 1991)). Also, the ratio of solute atoms to Al atoms in the clusters is not accurately known and hence we can only determine a proportionality of the volume fraction and fraction transformed:

$$f_{cl} \propto \alpha(c_0 - c_e) \tag{22}$$

where c_0 is the initial solute concentration in the matrix. Therefore, in this work, the value for $\Delta\mu$ was obtained by fitting the predicted yield strength to experimental yield strength data from a commercial 2024-T351 plate that was aged at 120°C and 170°C after long time natural ageing. The ageing curves showed a long plateau strength followed by a rise to the peak strength. The plateau strengths are attributed to the formation of Cu-Mg clusters. (In predicting the yield strengths of these 2024-T351 alloys, the contribution due to work hardening provided by the stretch in these alloys was calculated from the Ashby model (Ashby 1966, Kamp *et al.* 2002) and measured work hardening of these alloys to be 35MPa.)

Included in the model is a description of solid solution strengthening, for which the increment in CRSS, $\Delta\tau_{SS}$, is given by:

$$\Delta\tau_{ss} = \sum k_j c_j^{2/3} \tag{23}$$

where c_j are the concentrations of the alloying elements in solid solution and k_j are the factors describing the strengthening due to the individual elements. The yield strength of the alloys is related to the total CRSS by factor M (sometimes referred to as the Taylor factor):

$$\sigma_y = \sigma_i + M(\Delta\tau_{ss}{}^q + \Delta\tau_{cl}{}^q)^{1/q} \tag{24}$$

where the superposition exponent q depends on the relative strengths of the two types of obstacle, and is supposed to lie between 1 and 2 (Ardell 1985, Reppich 1993). When a few strong obstacles are mixed in with many weak obstacles q=1, whereas when two types of obstacles are of similar

strength q=2. If obstacles have strengths that differ up to about one order of magnitude, with both contributing significantly to the strength, q will be between 1 and 2.

In order to apply the model, a range of parameters are required as input data in the model, and all except for two can be identified of the basis of our experimental data and literature data. The intrinsic strength of the matrix σ_i is assumed to be constant throughout and consists of the yield strength for pure aluminium and the contribution from grain boundary strengthening. From data on commercial-purity unalloyed Al (Davis 1993), σ_i is estimated as 40MPa. Work on self-consistent modelling of the deformation of texture–free polycrystalline Al indicates that on average about 3.5 slip systems are activated per grain and this leads to M=2.6 (Clausen *et al*. 1998). To model the room temperature strengthening, we used the values for kinetic parameters σ_s, n and η_i determined in section 4.1, and E_{eff} (Al-1.2Cu-1.2Mg)=0.75kJ mol^{-1} (as determined in section 4.1) to calculate the amount of clusters formed. The solvus of clusters was considered to be given by a regular solution model (Starink and Wang 2003) and the solvus was fixed using data from Beton and Rollason (Beton and Rollason 1957-58). Solution strengthening factors k_j were fixed by considering yield strength data on Al-Cu and Al-Mg based solution-strengthened alloys (Davis 1993). We fitted $\Delta\mu$ and q to obtain the best fit of the room temperature hardening data and the yield strength data from a commercial 2024-T351 plate that was aged at 120°C and 170°C after long time natural ageing. Applying the combined kinetics and strengthening model, the best fit was found for q = 1.4. However varying the value of q between 1.3 and 1.6 did not have a significant influence on accuracy of model predictions.

The comparison between model prediction and experimental data for room temperature hardening is presented in figure 11 (The yield strength in MPa is taken as 2.3 times the Vickers hardness value

(Starink *et al*. 2002)). Also included is additional strength data of the 2024 alloy aged at 120°C and 170°C that was used to determine $\Delta\mu_{cl}$. A reasonably good agreement between experimental data and model predictions is observed. The small discrepancies in the very early stages may be due to the fact that we neglected the contribution by the Cu-clusters, which the APFIM revealed to be present at that stage. The good results obtained with the above model incorporating classical nucleation and growth of the clusters and modulus hardening due to their presence show that the rapid hardening in our Al-Cu-Mg alloys can be described entirely by a model based on modulus hardening by Cu-Mg clusters, with only two parameters being fitted. The fitted value of the superposition exponent q (1.4) is entirely reasonable considering that the two types of obstacles (clusters and solute atoms) have obstacle strengths and number densities that differ by about one order of magnitude, which means that q is smaller than 2, but differences are not as large to expect that q is close to unity. The fitted value of μ_{cl} depends to a limited extend on the amount of Al assumed to be present in the clusters, but all μ_{cl} values are within a range that is broadly consistent with published work. For instance, taking Al contents in clusters of 77 to 92% (where the higher Al content is obtained from the higher bound estimate from APFIM data in section 3.2) the fitted model would predict the shear modulus of the clusters to be 29 to 31GPa, which compares to an estimate of about 26.5 to 27.5 GPa based on a rule of mixtures (equation (21), using μ_{Al} = 26 GPa, μ_{Cu} = 48.3 GPa, μ_{Mg} = 17.3 GPa). The good agreement indicates that μ_{cl} obtained in the fitted model is reasonable. It is, however, equally clear that due to the small difference between μ_{Al} and μ_{cl}, accurate predictions of $\Delta\mu_{cl}$ with the rule of mixtures is not possible.

[Insert figure 11 above here]

To fully verify the present analysis of strengthening, and any future model attempting to predict strengthening due to clusters, the obstacle strength of a single cluster would need to be determined by measuring or predicting the effective μ_{cl} to a high accuracy (in the order of 1% or better). However, no such analysis is available at present, and the present quantitative analysis that relies on fitting of μ_{cl} is thought to currently provide the best basis for predicting the room temperature hardening in commercial purity Al-Cu-Mg alloys. The model is currently applied as part of a process model for age hardening and for welding of Al-Cu-Mg based alloys. In the latter case the present model is essential in predicting the hardness in regions of the weld that have experienced considerable dissolution of precipitates and which age harden (due to formation of co-clusters) during the final stages of the cooling after the weld thermal cycle (Starink *et al.* 2005).

4. Conclusions

Room temperature age hardening mechanisms of commercial purity Al-1.2Cu-1.2Mg-0.2Mn and Al-1.9Cu-1.6Mg-0.2Mn (at%) alloys were studied by hardness testing, DSC, isothermal calorimetry and 3DAP analysis. In the two alloys, hardening at room temperature occurs between about 0.5h and 20h at room temperature, and subsequently hardness remains constant. 3DAP analysis showed that after a short time of natural ageing Cu-rich clusters are present, and on further room temperature ageing Cu-Mg clusters form. During the room temperature hardening, the density of clusters increases and the Cu:Mg ratio in the clusters approaches unity. DSC and isothermal calorimetry shows that the formation of Cu-Mg clusters coincides with a substantial exothermic heat release. The microstructural analysis shows that the formation of Cu-Mg clusters coincides with the rapid hardness increase during natural ageing. The kinetics of cluster formation is analysed, and the results indicate that, even though the kinetics of Cu-Mg cluster formation will involve detailed

atomistic interactions, it can be described well as a classical nucleation and growth process. It is also shown that the yield strength (converted from hardness data) of these two alloys can be accurately described by a model incorporating modulus hardening originating from the difference in modulus between Al and Cu-Mg clusters and solution strengthening.

Acknowledgements

The authors would like to acknowledge the financial support from QinetiQ, EPSRC (grants GR/M95868/01 and GR/R10790/01) and Airbus UK for parts of this work.

References

Ardell, A. J., 1985, *Metal. Trans A*, **16**, 2131.

Ashby, M. F., 1966, *Philosph Mag*., **14**, 1157.

Avrami, M., 1939, *J Chem Phys*, **7**, 1103.
Avrami, M., 1940, *J Chem Phys*, **8**, 212.

Avrami, M., 1941, *J Chem Phys*, **9**, 177.

Beatrice, C. R. S., Garlipp, W., Cilense, M., and Adorno, A. T., 1995, *Scripta Mater*., **32**, 23.

Beton, R. H., and Rollason, E. C., 1957-58, *J Inst Met*., **86**, 77.

Cartaud, L., Guillot, and J., Grilhe, J., 1976, *Proceedings of 4th International Conference on the Strength of Metals and Alloys*, Vol. 1 (Nancy, France) pp. 214-218.

Charai, A., Walther, T., Alfonso, C., Zahra, A. M., and Zahra, C. Y., 2000, *Acta Mater*., **48**, 2751.

Christian, J. W., 1975, *Theory of Phase Transformations in Metals and Alloys* (Oxford: Pergamon Press).

Clausen, B., Lorentzen, T., and Leffers, T., 1998, *Acta Mater*., **46**, 3087.

Cumbrera, F. L., and Sanchez-Bajo, F., 1995, *Thermochim Acta*, **266**, 315.

Davin, L., 2004, PhD thesis, Oxford University.

Davis, J. R., 1993, *ASM Specialty Handbook: Aluminum and Aluminum Alloys* (ASM International).

Esmaeili, S., Lloyd, D. J., and Poole, W. J., 2003, *Acta Mater*., **51**, 2243.

Gao, N., Davin, L., Wang, S., Cerezo, A., and Starink, M. J., 2002, *Mater Sci Forum*, **396-402**, 923.

Gomiero, P., Brechet, Y., Louchet, F., Tourabi, A., and Wack, B., 1992, *Acta Metall*., **40**, 857.

Guo, X. Q., Podloucky, R., and Freeman, A. J., 1991, *J Mater Res*., **6**, 324.

Hardy, H. K., 1954-55, *J Inst Met*., **83**, 17.

Jena, A. K., Gupta, A. K., and Chaturvedi, M. C., 1989, *Acta Metall*., **37**, 885.

Kamp, N., Sinclair, I., and Starink, M. J., 2002, *Metall Trans A*, **33**, 1125.

Li, D., Gangloff, R. P., Bray, G. H., Galzov, M. V., and Rioja, R. J., 2001, *Advances in the Metallurgy of Al Alloys*, Proceeding of Materials Solutions Conference, edited by M. Tiryakioglu (Indianapolis, ASM International) p.105.

Liu, G., Zhang, G. J., Ding, X. D., Sun, J., and Chen, K. H., 2003, *Mater Sci. Eng. A*, **344**, 113.

Luo, A., Lloyd, D. J., Gupta, A., and Youdelis, W. V., 1993, *Acta Metall*., **41**, 769.

Miller, M. K., and Smith, G. D., 1989, *Atom Probe Microanalysis: Principles and Application to Materials Problems* (Materials Res. Soc.).

Miller, M. K., 2000, *Atom Probe Tomography: Analysis at the Atomic Level* (New York: Kluwer Academic). p. 159.

Nagai, Y., Murayama, M., Tang, Z., Nonaka, T., Hono, K., and Hasegawa, M., 2001, *Acta Mater*., **49**, 913.

Nembach, E., 1983, *Phys. Stat Sol A*, **79**, 571.

Nembach, E., 1996, *Particle Strengthening of Metals and Alloys*, Wiley, New York.

Ozbilen, S., and Flower, H. M., 1989, *Acta Metall.*, **37**, 2993.

Rajan, T. V., 1973, *Trans Indian Inst Met*., **26**, 72.

Reppich, B., 1993, *Particle Strengthening*, Vol. 6, edited by R. W. Cahn, P. Haasen and E. J. Kramer (Materials Science and Technology, VCH Verlagsgesellschaft mbH, Weinheim) p.311.

Ratchev, P., Verlinden, B., De Smet, P., and Van Houtte, P., 1998, *Acta Mater*., **46**, 3523.

Ratchev, P., Verlinden, B., De Smet, P., and Van Houtte, P., 1999, *Mater Trans. JIM*, **40**, 34.

Raviprasad, K., Hutchinson, C. R., Sakurai, T., and Ringer, S. P., 2003, *Acta Mater*., **51**, 5037.

Reich, L., Ringer, S. P., and Hono, K., 1999, *Philos Mag Lett*., **79**, 639.

Ringer, S. P., Hono, K., Polmear, I. J., and Sakurai, T., 1996, *Acta Mater*., **44**, 1883.

Ringer, S. P., Hono, K., Sakurai, T., and Polmear, I. J., 1997, *Scripta Mater*., **36**, 517.

Ringer, S. P., Sakurai, T., and Polmear, I. J., 1997, *Acta Mater*., **45**, 3731.

Robson, J.D., Jones, M.J., and Prangnell, P.B., 2003, *Acta Mater.*, **51**, 1453

Russell, K.C., 1970, in: H. I. Aaronson (Ed.), *Phase Transformations* (Am. Soc. Metals, Metals Park, Ohio) p. 219.

Sessa, V., Fanfoni, M., and Tomellini, M., 1996, *Phys Rev B*, **54**, 836.

Silcock, J. M., 1960-61, *J Inst Met.*, **89**, 203.

Sato, T., 2000, *Mater Sci Forum*, **331-337**, 85.

Starink, M. J., 1996, *Thermochim Acta*, **288**, 97.

Starink, M. J., and Zahra, A. M., 1997, *Thermochim Acta*, **292**, 159.

Starink, M. J., and Zahra, A. M., 1997, *Thermochim Acta*, **298**, 179.

Starink, M. J., and Zahra, A. M., 1998, *Acta Mater*., **46**, 3381.

Starink, M. J., and Zahra, A. M., 1998, *Philos Mag A*, **77**, 187.

Starink, M. J., Zahra, C. Y., and Zahra, A. M., 1998, *J Therm Anal*., **51**, 933.

Starink, M. J., Wang, P., Sinclair, I., and Gregson, P. J., 1999, *Acta Mater*., **47**, 3841.

Starink, M. J., Wang, P., Sinclair, I., and Gregson, P. J., 1999, *Acta Mater*., **47**, 3855.

Starink, M. J., 2001, *J Mater Sci*., **36**, 4433.

Starink, M. J., Sinclair, I., Gao, N., Kamp, N., Gregson, P. J., Pitcher, P. D., Levers, A., and Gardiner, S., 2002, *Mater Sci Forum*, **396-402**, 601.

Starink, M. J., 2003, *Thermochim Acta*, **404**, 163.

Starink, M. J., and Wang, S. C., 2003, *Acta Mater*., **51**, 5131.

Starink, M. J., 2004, *International Mater Rev.*, **49**, 191.

Starink, M. J., Gao, N., and Yan, J. L., 2004, *Mater Sci Eng A*, in press.

Starink, M. J., Wang, S. C., and Sinclair I., 2005, in *Friction stir welding and processing III*, edited by K. V. Jata, M. W. Mahoney, R. S. Mishra and T. J. Lienert, in press.

Takahashi, T., and Sato, T., 1985, *J Jpn Inst Light Metals*, **35**, 41.

Vaumousse, D., Cerezo, A., and Warren, P. J., 2003, *Ultramicroscopy*, **95**, 215.

Vietz, J. T., and Polmear, I. J., 1966, *J Inst Met*., **94**, 410.

Yan, J. L., Starink, M. J., Gao, N., and Yan, J. L., 2004, unpublished research.

Zahra, A. M., Zahra, C. Y., Alfonso, C., and Charai, A., 1998, *Scripta Mater.,* **39**, 1553.

Zahra, A. M., Zahra, C. Y., Lacom, W., and Spiradek, K., 1990, Proc. of the Int. Conf. on Light Metals, edited by T. Khan and G. Effenberg (Amsterdam, ASM International) p. 633.

Tables

Table 1: Compositions of the alloys (at.%)

Alloy	Cu	Mg	Mn
Al-1.2Cu-1.2Mg	1.21	1.19	0.21
Al-1.9Cu-1.6Mg	1.89	1.56	0.21

Figures

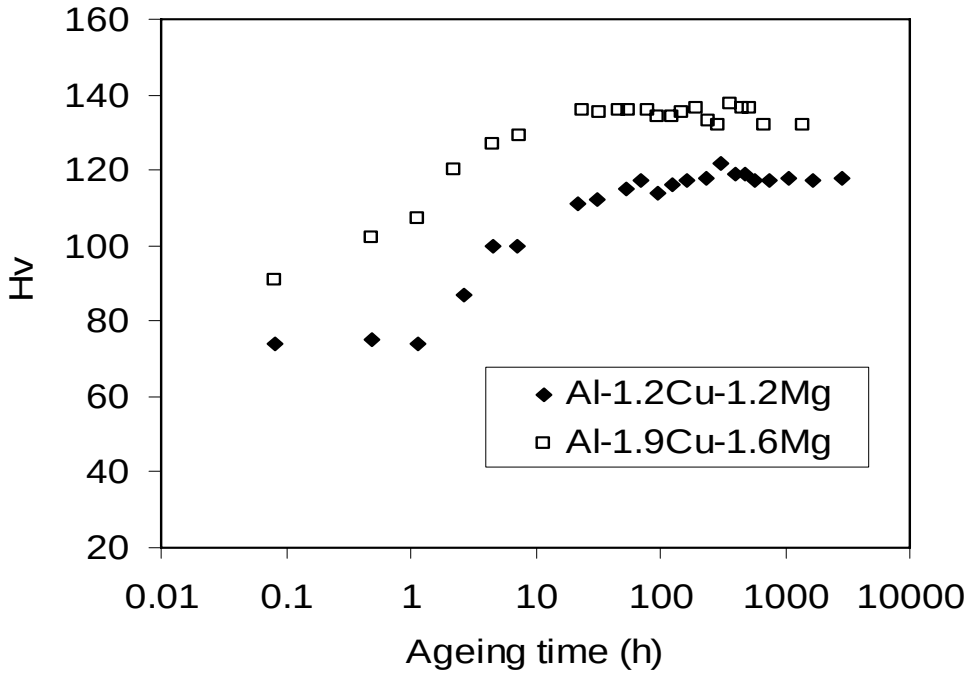

Fig. 1 Age hardening of the Al-1.2Cu-1.2Mg and the Al-1.9Cu-1.6Mg alloy at 25ºC

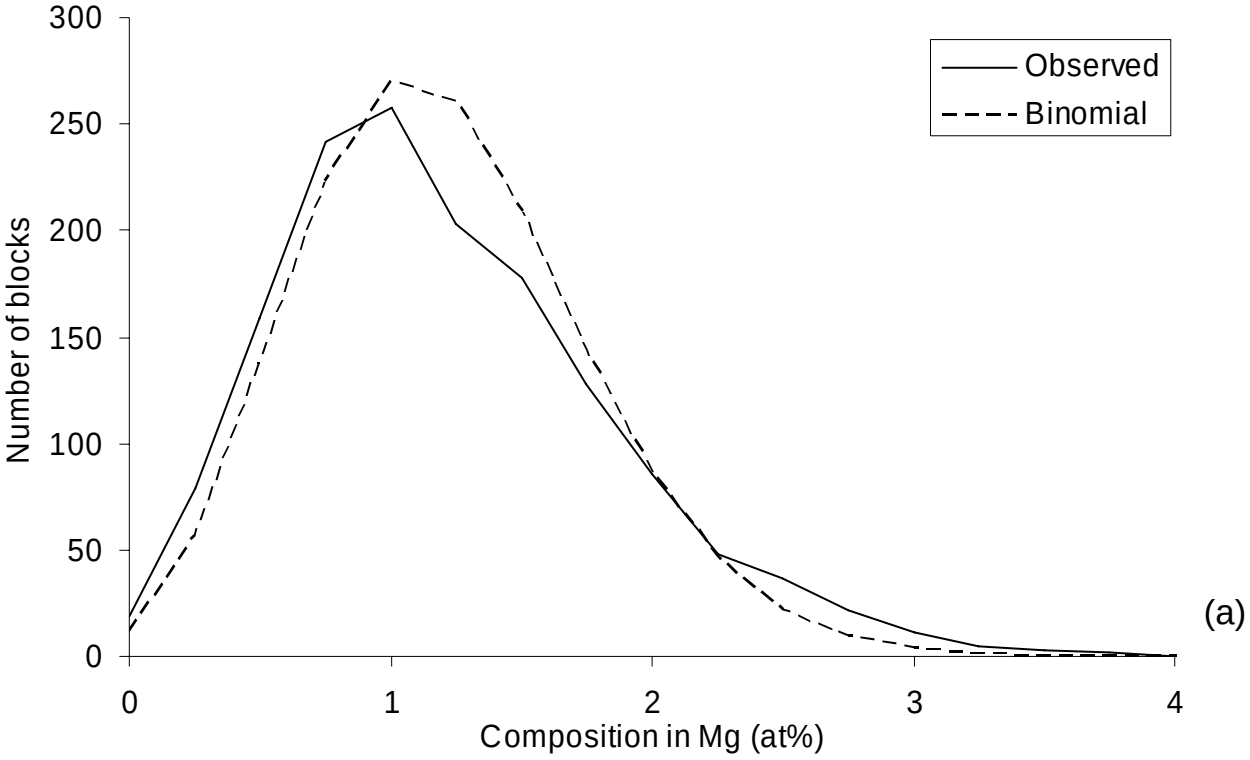
300
250
200
150
100
50
0
Number of blocks
0
1
2
3
4
Composition in Mg (at%)
Observed
Binomial
(a)

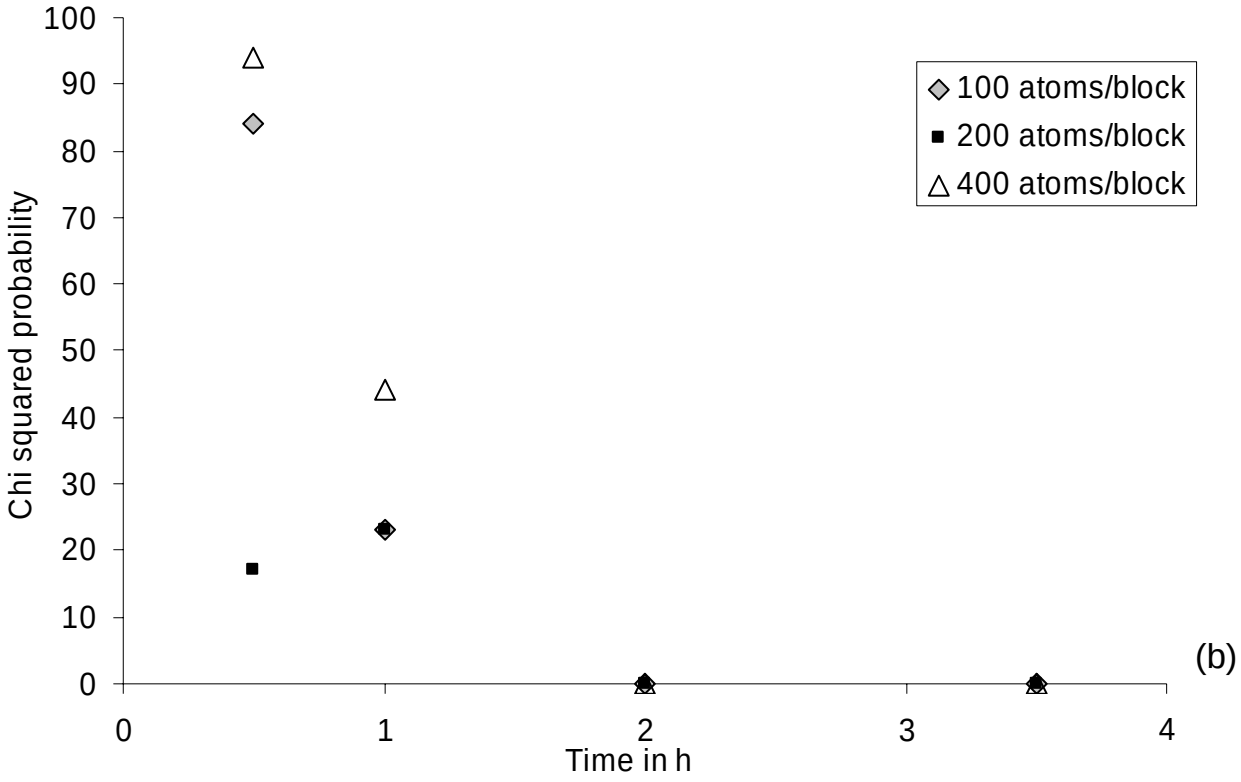

Fig. 2 a) Mg frequency distribution (observed and binomial) curves of Al-1.2Cu-1.2Mg alloy aged for 2h at 25ºC with a total number of atoms per block of 400. b) Result of the χ^2 test on the frequency distribution of Mg atoms in the Al-1.2Cu-1.2Mg alloy aged up to 3.5 h at 25ºC and variable number of atoms per blocks.

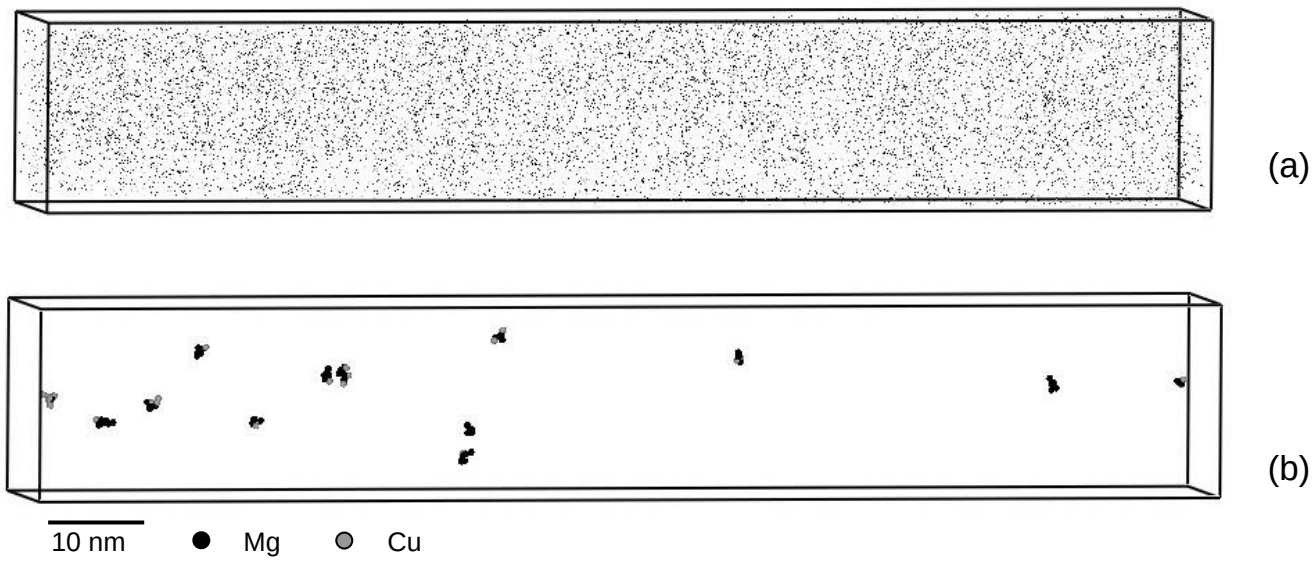

Fig. 3 Three dimensional atom map representing the distribution of the Mg and Cu atoms in the Al-1.2Cu-1.2Mg alloy aged at 25ºC for 2h before (a) and after (b) selection of the clusters (the size of the atoms has been increased in fig.3(b) to make the clusters more visible but in both cases it is not proportional to the size of the atoms)

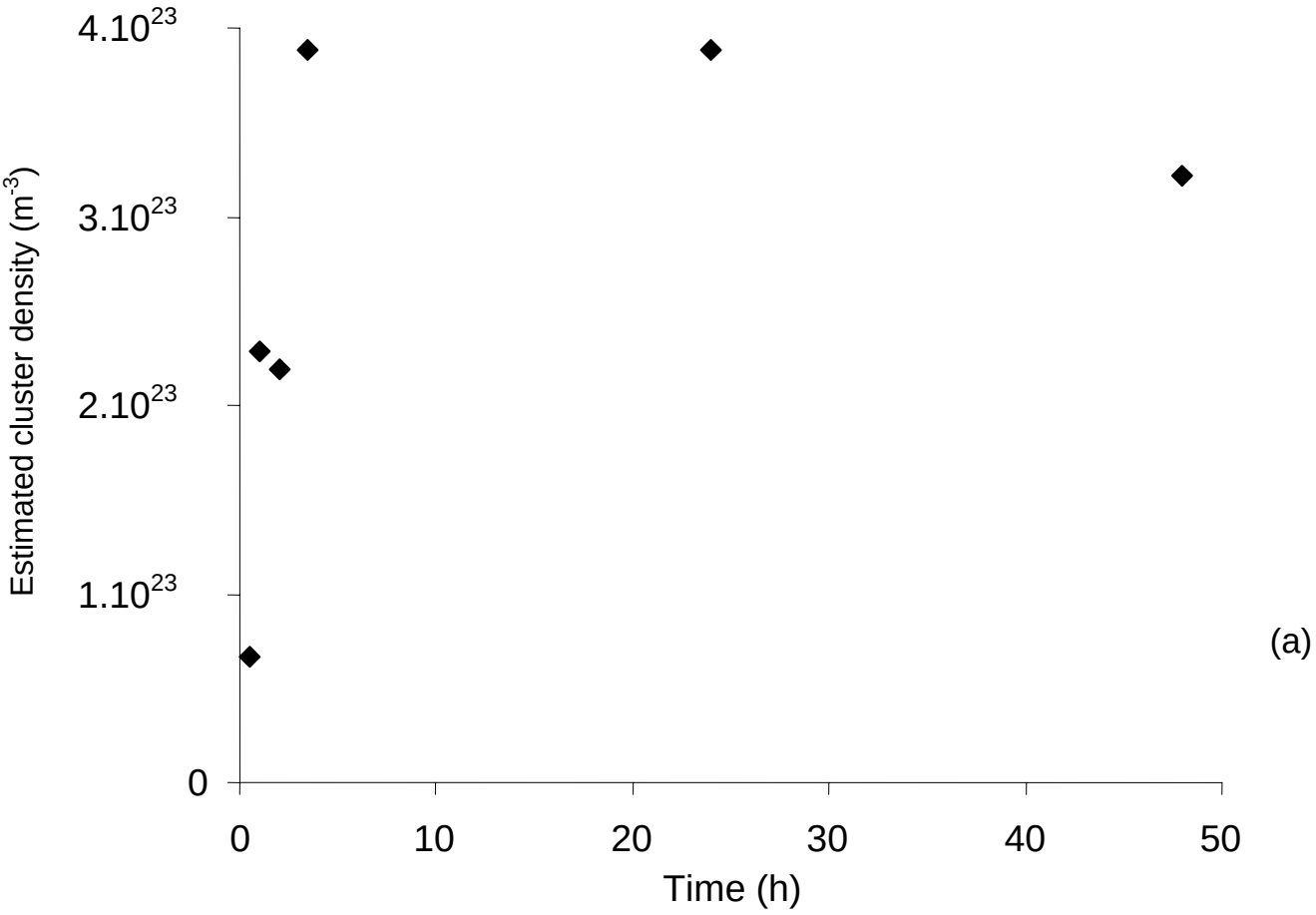
4.10^23
3.10^23
2.10^23
1.10^23
0
Estimated cluster density (m^-3)
0
10
20
30
40
50
Time (h)

(a)

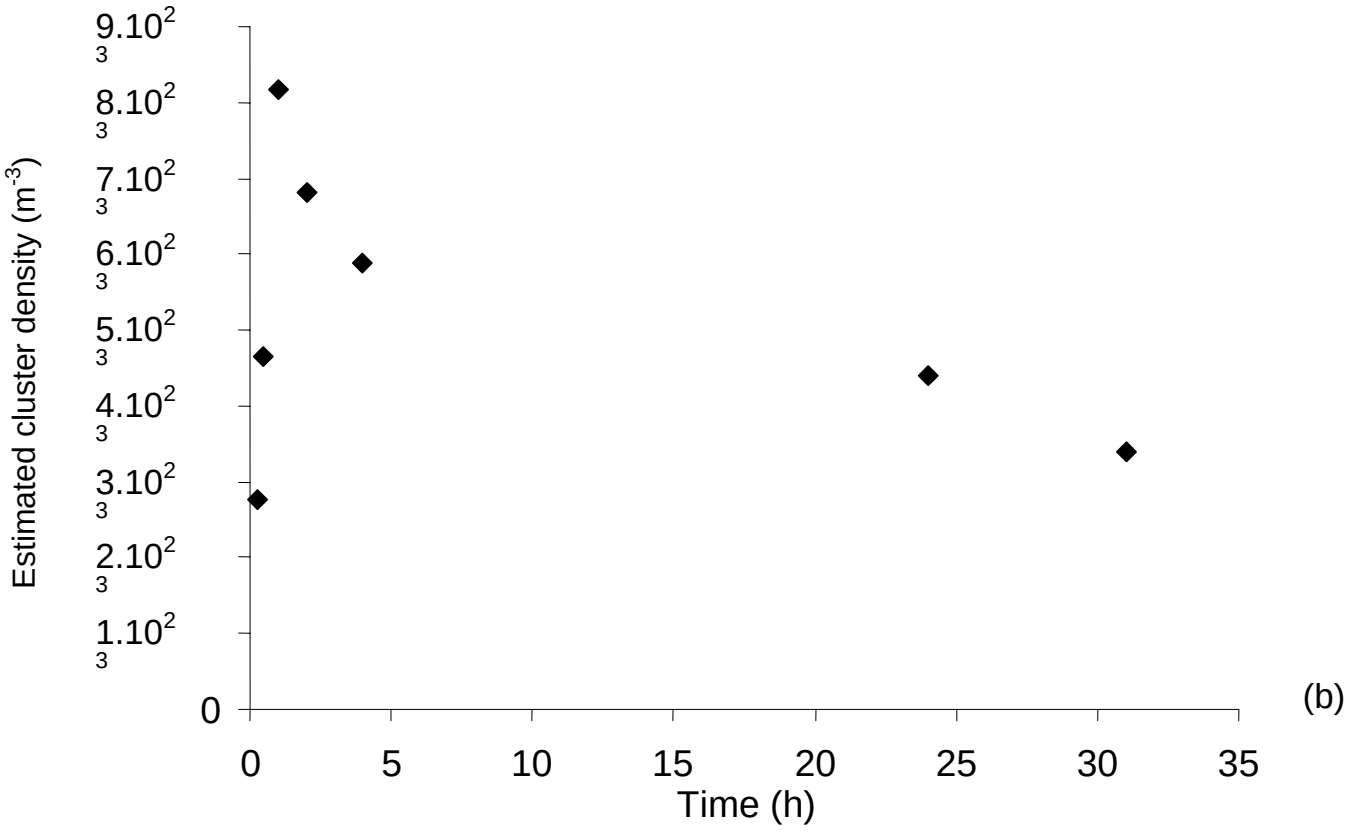

Fig. 4 Estimated cluster density (per m^3) during ageing at 25ºC for (a) the Al-1.2Cu-1.2Mg alloy (b) the Al-1.9Cu-1.6Mg alloy

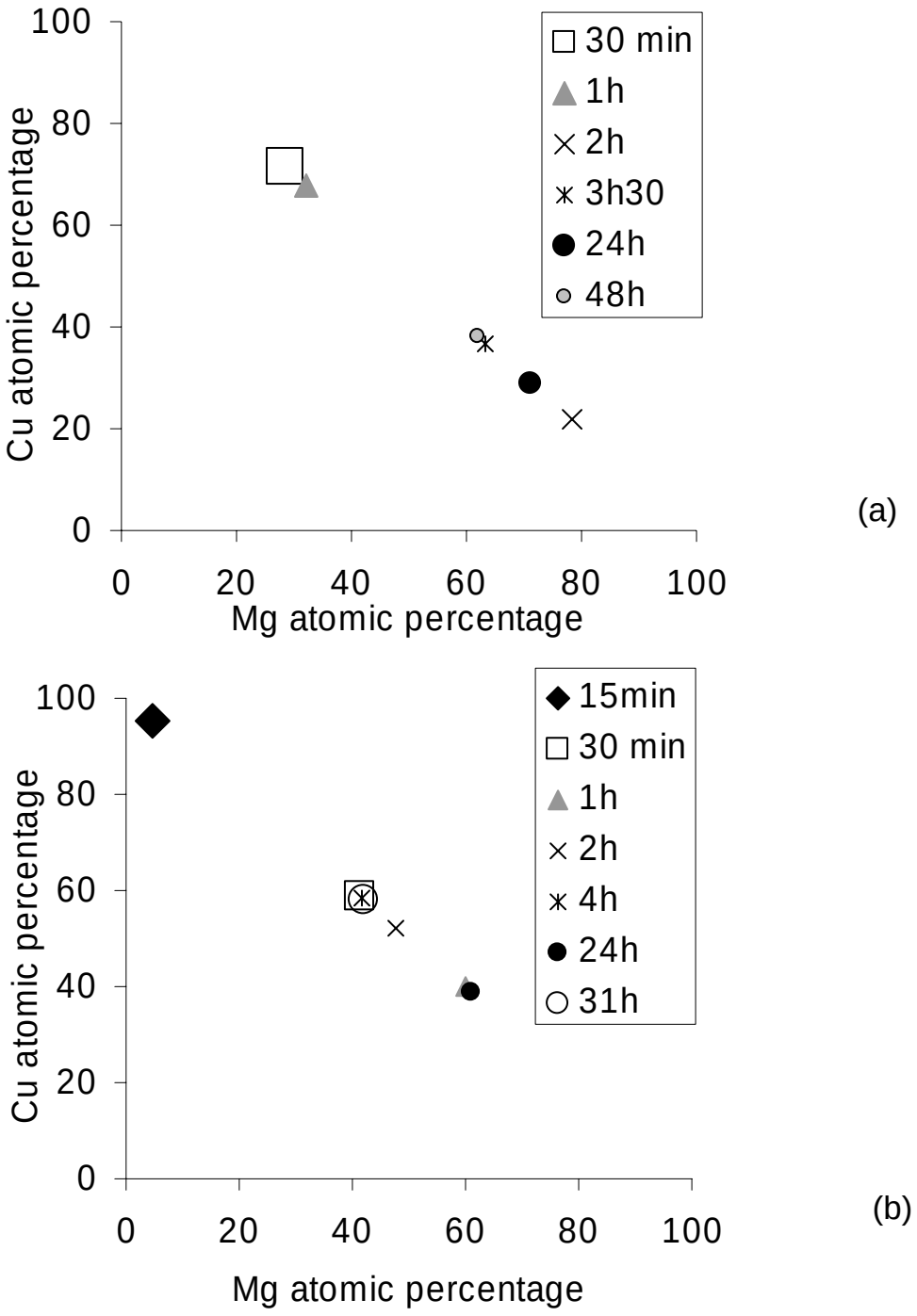

Fig. 5 (a)Average composition of clusters in the Al-1.2Cu-1.2Mg alloy during ageing at 25ºC. (b)Average composition of clusters in the Al-1.9Cu-1.6Mg alloy during ageing at 25ºC. (The size of the symbols is proportional to the error)

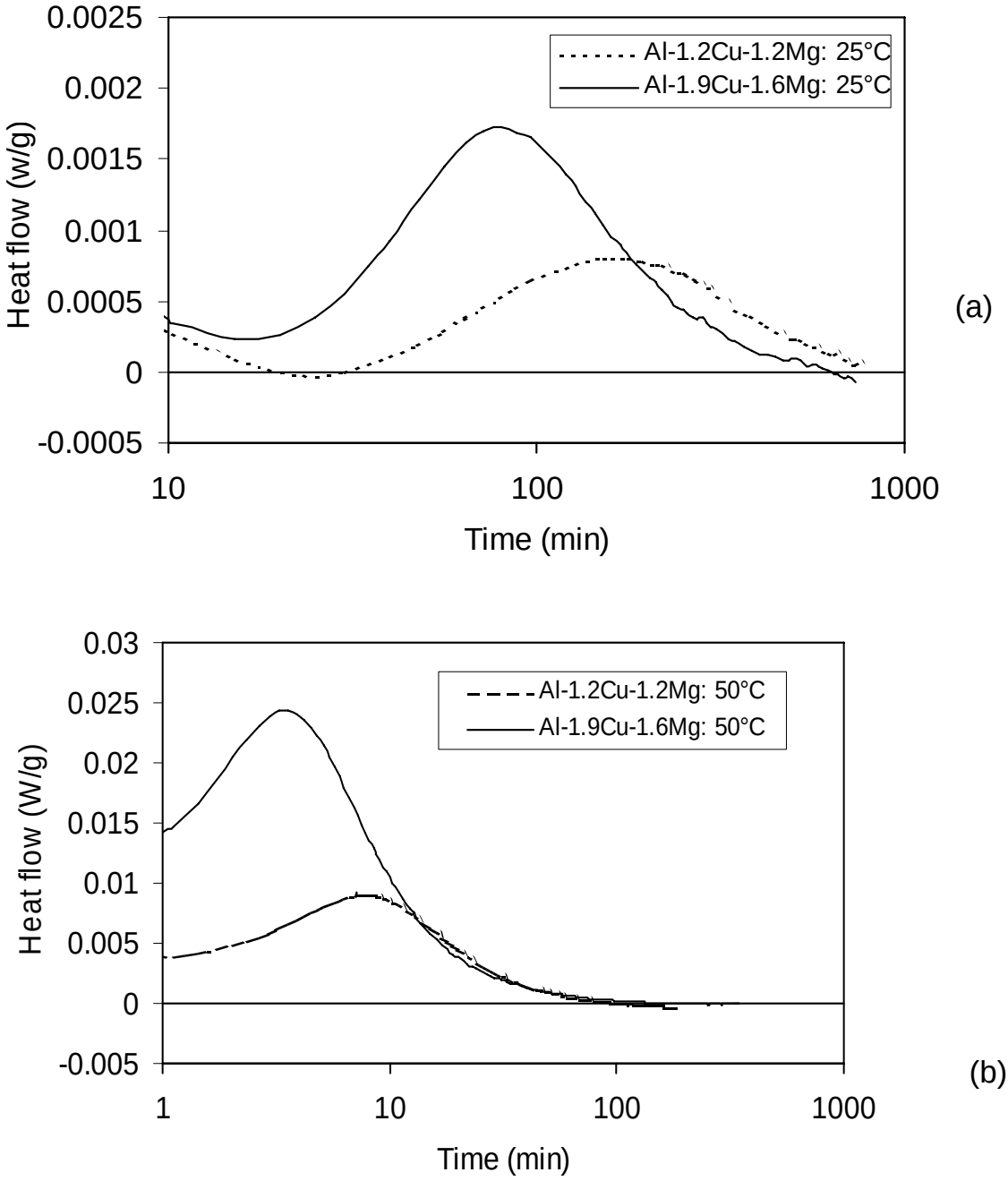

Fig. 6 Isothermal calorimetry curves of the Al-1.2Cu-1.2Mg and the Al-1.9Cu-1.6Mg alloy during ageing at (a) 25 and (b) 50ºC.

(a)

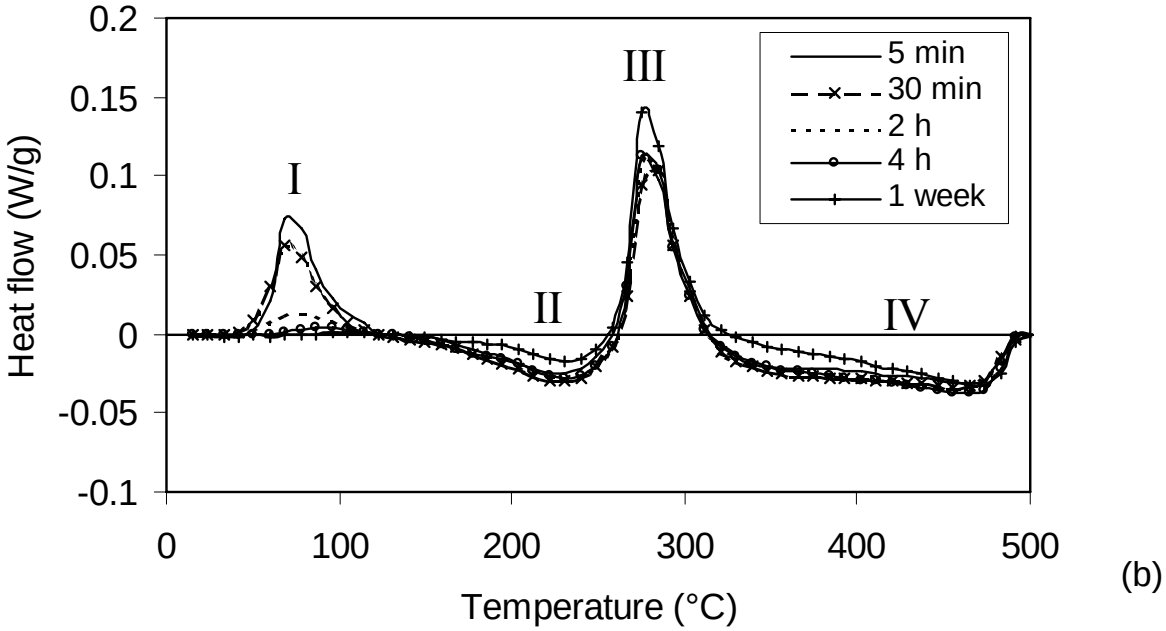

Fig. 7 DSC curves of the Al-1.9Cu-1.6Mg alloy after ageing for several intervals ageing at 25ºC.

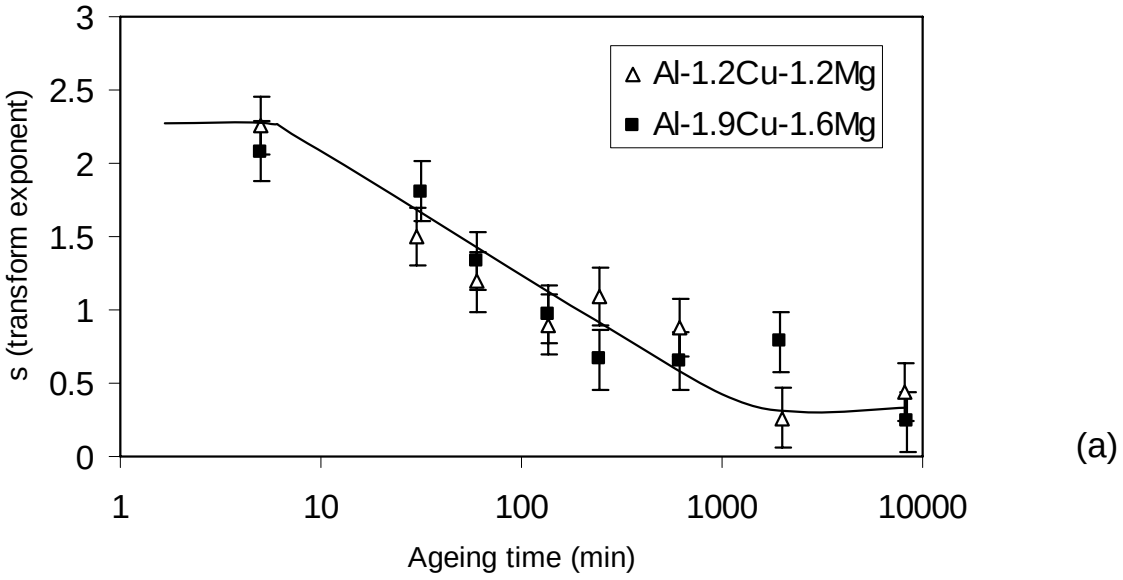

Fig. 8 Reaction exponent s for the Cu-Mg clustering effect as a function of the ageing time at 25ºC for the Al-1.2Cu-1.2Mg and the Al-1.9Cu-1.6Mg alloy.

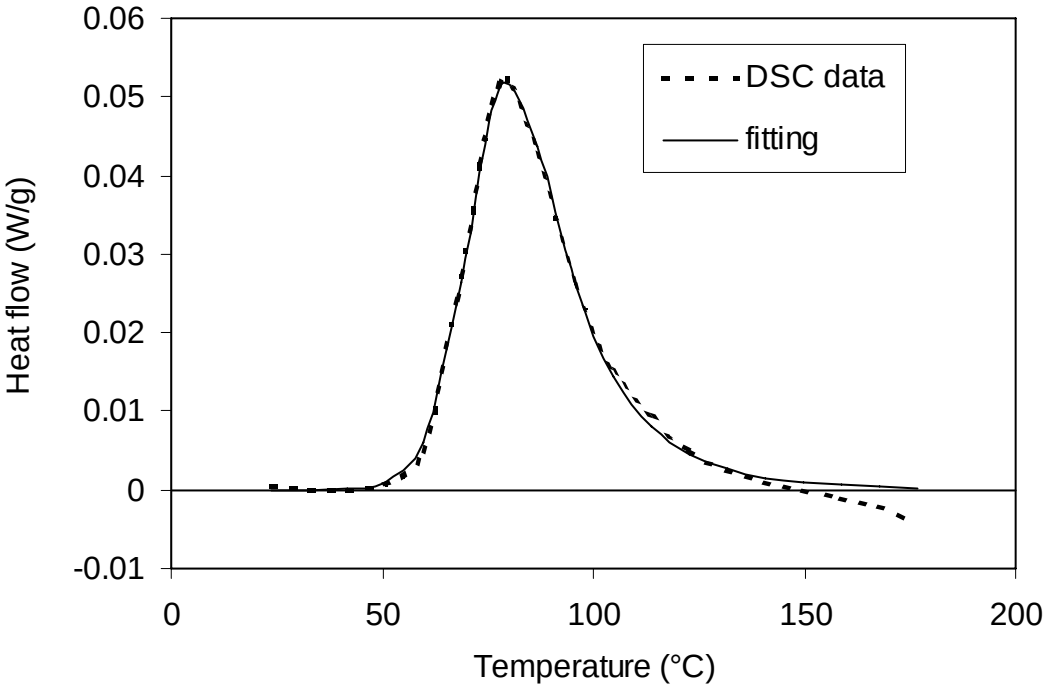

Fig. 9 Effect I in the DSC curve of the Al-1.2Cu-1.2Mg alloy aged for 5 minutes at 25ºC and a fit based on Eq.(3) and (6). Heating rate 10ºC/min.

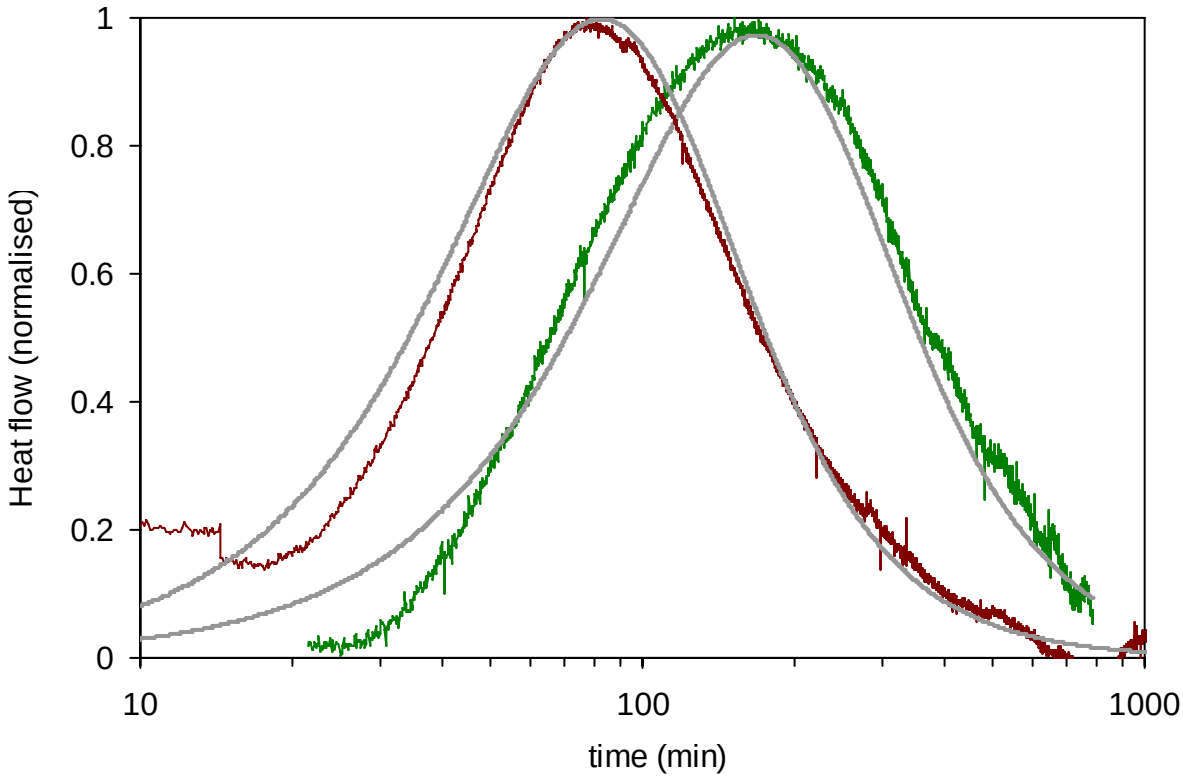

Fig 10 Isothermal calorimetry data on the heat flow due to cluster formation at 25ºC in the Al-1.2Cu-1.2Mg and the Al-1.9Cu-1.6Mg alloy (thin dark curves) compared with predictions from the model outlined in Section 4.1 (n=2.5, η_i=0.6, σ = 0.06J/m^2) (thicker, grey curves).

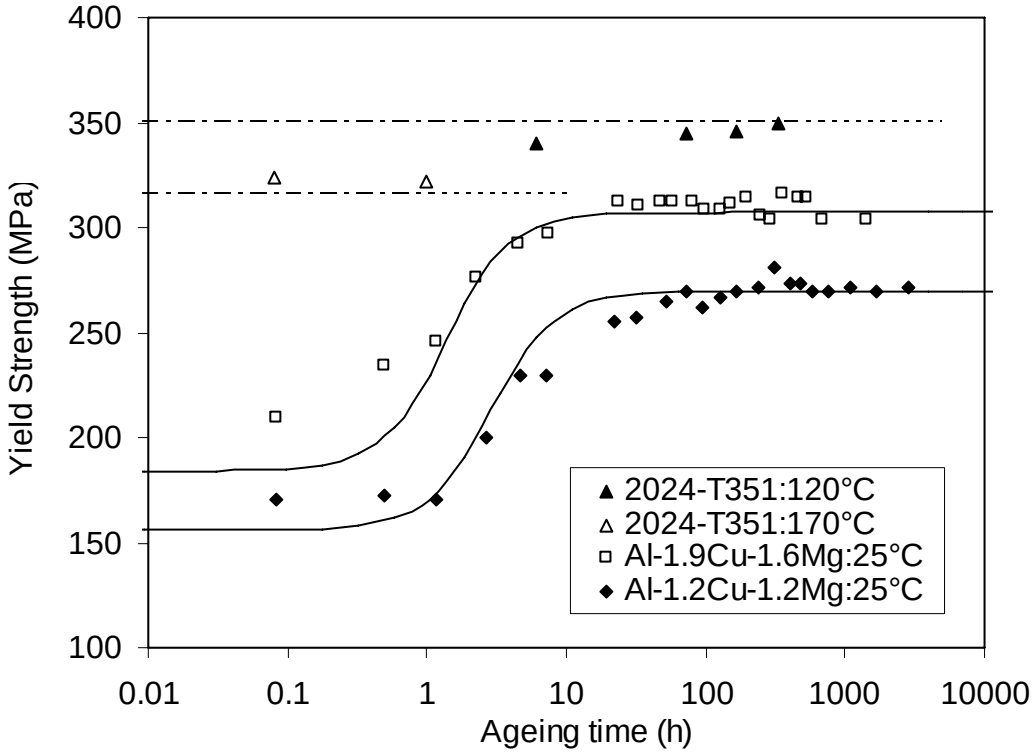

Fig. 11 Measured strengths of the Al-1.2Cu-1.2Mg and the Al-1.9Cu-1.6Mg alloy and modelling results.